3D numerical simulation of on ground Marangoni flow instabilities in liquid bridges of low Prandtl number fluid

M. Lappa
Dipartimento di Scienza e Ingegneria dello Spazio "Luigi G. Napolitano", Università degli Studi di Napoli "Federico II", Napoli, Italy
Microgravity Advanced Research and Support Center (MARS), Via Gianturco, Napoli, Italy
S. Yasushiro and N. Imaishi
Institute of Advanced Material Study, Kyushu University, Kasuga, Fukuoka, Japan

Received March 2002
Revised November 2002
Accepted November 2002

Keywords *Metals, Flow, Instability*

Abstract *The influence of gravity on the Marangoni flow instability in half zone liquid bridges in the case of liquid metals is investigated by direct 3D and time-dependent simulation of the problem. The computations are carried out for different heating conditions and environments (zero g conditions and on ground liquid zone heated from above or from below). The case of cylindrical shape (simplified model) and of melt/air interface deformed by the effect of gravity (real conditions) are considered. The comparison among these situations gives insight into the separate (gravity) effects of buoyancy forces and of the free surface deviation with respect to straight configuration. Body-fitted curvilinear co-ordinates are adopted to handle the non-cylindrical problem. The liquid bridge exhibits different behaviours according to the allowed bridge shape. If the shape is forced to be cylindrical, the flow field is stabilized in the case of heating from above and destabilized if gravity is reversed. If the deformation is taken into account, gravity always stabilizes the Marangoni flow regardless of its direction (parallel or antiparallel to the axis) and the 3D flow structure is different according to the heating condition (from above or from below). In the latter case, the critical Marangoni number is larger and the critical wave number is smaller, compared with the opposite condition. In addition, for Pr = 0.02 (Gallium), a surprising heretofore unseen behaviour arises. No steady bifurcation occurs and the flow becomes unstable directly to oscillatory disturbances. This phenomenon has never been reported before in the case of low Prandtl number liquids.*

Introduction

Marangoni convection in a half-zone liquid bridge of length L and radius R confined between two differentially heated isothermal solid disks has become

The present results have been obtained during the visit (March-April 2000) of Dr Marcello Lappa to the laboratories of Professor Nobuyuki Imaishi (Kyushu University, Japan). The authors would like to thank Dr B.-C. Sim and Professor A. Zebib(Rutgers University, New Jersey) and Dr V. Shevtsova (University of Bruxelles) for some helpful discussions about the body-fitted curvilinear co-ordinates and their application to the boundary conditions.

International Journal of Numerical Methods for Heat & Fluid Flow
Vol. 13 No. 3, 2003
pp. 309-340

0961-5539
DOI 10.1108/09615530310464526

over the years, a typical model for the study of Marangoni flows, their stability, and their bifurcations. The stability of free convection in non-isothermal liquid bridges with quasi-cylindrical free surfaces has been in fact the subject of intense research. These studies are motivated by the fact that flow instabilities in such configurations may be responsible for the appearance of undesirable striations in crystals grown by floating zone technique.

It is well known that the flow exhibits axi-symmetric and steady toroidal roll cell structure if the temperature difference between the two disks is small and that it becomes unstable and a 3D Marangoni flow arises when the applied temperature gradient exceeds a certain threshold value. On this subject, there have been many experimental works, theoretical studies by means of the linear stability analyses and non-linear numerical simulations.

Experiments (Frank and Schwabe, 1998; Preisser *et al.*, 1983; Velten *et al.*, 1991) performed with half zone liquid bridges of transparent liquids (with Prandtl numbers higher than those typical of liquid metals) have shown that 3D Marangoni flow always starts with oscillatory behaviour (Hopf bifurcation). The development of supercomputers and efficient numerical methods led the investigators to study the problem through direct numerical solution of the non-linear and time-dependent Navier Stokes equations. Levenstam and Amberg (1995), Leypoldt *et al.* (2000) and Rupp *et al.* (1989) found that for liquid metals, the first bifurcation is stationary (i.e. the supercritical 3D state is steady) and that the regime becomes oscillatory only if the Marangoni number is further increased (second oscillatory bifurcation). Lappa and Savino (1999) used parallel supercalculus to study the 3D structure (characterized by the appropriate value of the azimuthal wave number of the instability) of the flow pattern that is established after the steady bifurcation for $\mathrm{Pr} = 0.04$. Imaishi *et al.* (1999, 2000) and Yasushiro *et al.* (2000) depicted in detail the complex spatio-temporal behaviour of the flow field that occurs after the second (oscillatory) bifurcation of the Marangoni flow for different values of the aspect ratio (defined as ratio of the length and of the radius of the liquid bridge, i.e. $A = L/R$) and of the Prandtl number ($0 \leq \mathrm{Pr} \leq 0.02$), elucidating different oscillatory behaviours.

Lappa *et al.* (2001a) pointed out that for non-cylindrical (convex or concave) liquid bridges of liquid metal ($\mathrm{Pr} = 0.01$), the flow field and the critical wave number depend on the geometrical aspect ratio and also on the shape factor $S = V/V_0$ of the liquid bridge (V: volume of the liquid, V_0: volume of the cylinder having radius R and length L; liquid surface is convex for $S > 1$, concave for $S < 1$).

Since it is very difficult to conduct a well controlled experiment with liquid metals of small Prandtl numbers (due to opacity, reactivity and high temperatures of the melts), there are only few experiments on the flow instability in half zone liquid bridges of semiconductor materials. During on ground experimentation, sounding rocket missions and other parabolic flights,

using a X-ray radiography technique with zirconium-core tracers, Nakamura *et al.* (1998) investigated the supercritical Marangoni flow in a molten column of silicon.

To date, several numerical investigations in the case of high Prandtl number liquids have become available. Lappa *et al.* (2001b), Yasushiro *et al.* (1997, 1999) and Zeng *et al.* (1999) analysed the influence of the aspect ratio on the time-dependent 3D structure of Marangoni flow for $\mathrm{Pr} = 1$, 16 and 30, respectively, elucidating many features of the supercritical flow (e.g. the oscillation type, *standing wave* or *travelling wave*). Shevtsova and Melnikov (2000) extended these studies taking into account the influence of the temperature-dependent viscosity on the supercritical flow field for $1 < \mathrm{Pr} < 4$.

Linear stability analyses (Chen and Hu, 1998; Chen *et al.*, 1997, 1999; Kuhlmann and Rath, 1993; Neitzel *et al.*, 1992; Wanschura *et al.*, 1995) have confirmed that for high Prandtl number fluids, the instability is oscillatory (Hopf bifurcation) whereas for low Prandtl number fluids, the instability breaks the spatial axisymmetry (but the flow regime is still steady) prior to the onset of time dependent flow field (in this case, the instability is hydrodynamic in nature i.e. its mechanism does not involve a coupling between the temperature and the velocity disturbances). These analyses extended the investigated range of aspect ratios and values of the Prandtl number and elucidated that the 3D Marangoni flows are initiated through different mechanisms, i.e. inertia instability of the axial shear layer below the free surface for small Pr fluids and hydrothermal wave for large Pr fluid case.

Many studies also have appeared where the stability of the combined Marangoni buoyant convection was investigated. Excellent experiments have been given by Velten *et al.* (1991). They studied the influence of gravity (heating from above and heating from below) on the transition point, frequency and spatial structure of the flow field in the case $\mathrm{Pr} = 1$, 7 and 49. Using linear stability technique, Wanschura *et al.* (1997) considered the stability limit of combined buoyant-thermocapillary flow in half-zone liquid bridge for a fixed aspect ratio ($A = 1.0$) and $\mathrm{Pr} = 4$. A systematic and parametric analysis of the features of the mixed buoyancy-Marangoni instability for a high Prandtl liquid ($\mathrm{Pr} = 30$) over a large range of aspect ratios ($0.4 \leq A \leq 1.0$) was carried out through full 3D solution of the time-dependent, non-linear and complete Navier Stokes equations by Lappa *et al.* (2000).

Surface deformation due to the gravity field was neglected in the above theoretical and numerical studies, since only low values of the aspect ratio were investigated ($A \leq 1.0$). The experimental results (Velten *et al.*, 1991), the theoretical studies by means of the linear stability analyses (Wanschura *et al.*, 1997) and non-linear numerical simulations (Lappa *et al.*, 2000) have shown, in the case of high Prandtl number liquids, that the critical wave number in azimuthal direction at the onset of instability completely changes according to whether the bridge is heated from above or from below

and that the Marangoni flow is strongly stabilized under the heating-from-below condition.

In spite of the large theoretical and numerical efforts done to study the gravity effect on the features of the Marangoni flow instability, in the case of high Prandtl liquids, no work has appeared in literature investigating this problem for liquid metals. Aim of the present paper is to extend the analysis to low Prandtl number cases and to larger aspect ratio where the deformation of the free surface due to gravity cannot be neglected. These amphoral shape provide more accurate simulations of the on-ground floating zone experiments.

Physical and mathematical model

Basic assumptions

The geometry of the problem is shown in Figure 1. An axi-symmetric liquid bridge of length L and diameter D is held between two coaxial disks at different temperatures. The upper disk in Figure 1 is kept at the temperature $\bar{T}_H$ higher than the temperature $\bar{T}_C$ of the lower cold disk. The imposed temperature difference is denoted by $\overline{\Delta T}$ ($\bar{T}_H = \bar{T}_C + \overline{\Delta T}$). The overbar denotes dimensional quantities. The liquid is assumed to be homogeneous and Newtonian, with constant density and constant coefficients; viscous dissipation is negligible. The liquid filling the bridge is bounded by an axi-symmetric liquid-gas interface with a surface tension $\bar{\sigma}$ exhibiting a linear decreasing dependence on the temperature:

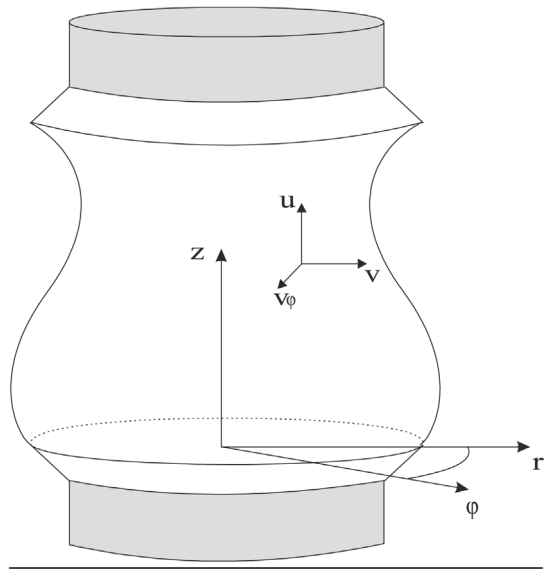

Figure 1.
Sketch of the liquid bridge

$$\bar{\sigma} = \bar{\sigma}_{\mathrm{o}} - \bar{\sigma}_T(\bar{T} - \bar{T}_{\mathrm{C}}) \tag{1}$$

where $\bar{\sigma}_{\mathrm{o}}$ is the surface tension at $\bar{T} = \bar{T}_{\mathrm{C}}$ and $\bar{\sigma}_T = -\mathrm{d}\bar{\sigma}/\mathrm{d}\bar{T} > 0$.

Since it is well known that experimental dynamic interface deformations are negligible (10^{-6} m) compared to the floating zone size (10^{-2} m), it can be assumed that dynamic deformations do not significantly influence the features of the Marangoni flow instability investigated for static shapes. For this reason, the interface is assumed to be non-deformable and axi-symmetric around the z-axis; its radial co-ordinate is a function of the $\bar{z}$ variable ($\bar{r} = \bar{c}(\bar{z})$). The hydrostatic shape of this surface can be obtained from the Gauss-Laplace equation, relating the local curvature of the surface to the pressure jump along the liquid-gas interface:

$$\overline{\Delta p} + \bar{\rho} g \bar{z} = \bar{\sigma}\left(\frac{1}{R_1} + \frac{1}{R_2}\right) \tag{2}$$

where R_1 and R_2 are the principal radii of curvature at each point of the surface.

Equation (2) may be reformulated in dimensionless form in the cylindrical co-ordinates by substituting the analytical expression of the principal radii of curvature in axi-symmetric geometry in terms of the surface equation $c(z)$ ($c = \bar{c}/L$, $r = \bar{r}/L$, $z = \bar{z}/L$) :

$$\frac{1}{c(1 + c'^2)^{1/2}} - \frac{c''}{(1 + c'^2)^{3/2}} = \frac{L\overline{\Delta p}}{\bar{\sigma}} + \frac{\overline{\rho g} L^2}{\bar{\sigma}} z = k_1 + k_2 z \tag{3}$$

The parameter $k_2 = L^2\overline{\rho g}/\bar{\sigma}$ takes into account the deformation of the shape under gravity conditions. It depends on the value of the g-level, on the length of the liquid bridge and on the properties of the liquid under investigation ($\bar{\rho}$ and $\bar{\sigma}$). Each value of the parameter $k_1 = L\overline{\Delta p}/\bar{\sigma}$ corresponds to a fixed volume of the liquid bridge. For the present analysis, the value of k_1 has been assigned in equation (3) in order to obtain a volume V equal to $V_0 = \pi R^2 L$ (i.e. $V/V_0 = 1$) and the equation has been integrated by a shooting method with the conditions that the liquid is attached to the solid supports:

$$c(0) = c(1) = R/L \tag{4a, b}$$

Non-dimensional field equations and boundary conditions

The flow is governed by the continuity, Navier-Stokes and energy equations, that in non-dimensional conservative form (cylindrical co-ordinates) read:

$$\frac{\partial u}{\partial z} + \frac{\partial v}{\partial r} + \frac{v}{r} + \frac{1}{r}\frac{\partial V_\phi}{\partial \phi} = 0 \tag{5a}$$

$$\frac{\partial u}{\partial t} = -\frac{\partial p}{\partial z} - \left(\frac{\partial u^2}{\partial z} + \frac{\partial uv}{\partial r} + \frac{uv}{r} + \frac{1}{r}\frac{\partial uV_\phi}{\partial \phi}\right) + \mathrm{Pr}\left(\frac{\partial^2 u}{\partial z^2} + \frac{\partial^2 u}{\partial r^2} + \frac{1}{r}\frac{\partial u}{\partial r} + \frac{1}{r^2}\frac{\partial^2 u}{\partial \phi^2}\right) - \mathrm{Pr}\,\mathrm{Ra}T \tag{5b}$$

$$\frac{\partial v}{\partial t} = -\frac{\partial p}{\partial r} - \left(\frac{\partial uv}{\partial z} + \frac{\partial v^2}{\partial r} + \frac{v^2}{r} + \frac{1}{r}\frac{\partial vV_\phi}{\partial \phi} - \frac{V_\phi^2}{r}\right) + \mathrm{Pr}\left(\frac{\partial^2 v}{\partial z^2} + \frac{\partial^2 v}{\partial r^2} - \frac{v}{r^2} + \frac{1}{r}\frac{\partial v}{\partial r} + \frac{1}{r^2}\frac{\partial^2 v}{\partial \phi^2} - \frac{2}{r^2}\frac{\partial V_\phi}{\partial \phi}\right) \tag{5c}$$

$$\frac{\partial V_\phi}{\partial t} = -\frac{1}{r}\frac{\partial p}{\partial \phi} - \left(\frac{\partial uV_\phi}{\partial z} + \frac{\partial vV_\phi}{\partial r} + \frac{2vV_\phi}{r} + \frac{1}{r}\frac{\partial V^2}{\partial \phi}\right) + \mathrm{Pr}\left(\frac{\partial^2 V_\phi}{\partial z^2} + \frac{\partial^2 V_\phi}{\partial r^2} + \frac{1}{r}\frac{\partial V_\phi}{\partial r} - \frac{V_\phi}{r^2} + \frac{1}{r^2}\frac{\partial^2 V_\phi}{\partial \phi^2} + \frac{2}{r^2}\frac{\partial v}{\partial \phi}\right) \tag{5d}$$

$$\frac{\partial T}{\partial t} = -\left(\frac{\partial uT}{\partial z} + \frac{\partial vT}{\partial r} + \frac{vT}{r} + \frac{1}{r}\frac{\partial uV_\phi}{\partial \phi}\right) + \left(\frac{\partial^2 T}{\partial z^2} + \frac{\partial^2 T}{\partial r^2} + \frac{1}{r}\frac{\partial T}{\partial r} + \frac{1}{r^2}\frac{\partial^2 T}{\partial \phi^2}\right) \tag{5e}$$

where V, p and T are the non-dimensional velocity, pressure and temperature, Pr is the Prandtl number (defined by $\mathrm{Pr} = \nu/\alpha$ where ν is the kinematic viscosity and α is the thermal diffusivity). The Rayleigh number is defined by $\mathrm{Ra} = \frac{g\beta_T \Delta T L^3}{\nu\alpha}$ where β_T is the thermal expansion coefficient. The non-dimensional form results from scaling the cylindrical co-ordinates ($\bar{z}$, $\bar{r}$) by the axial distance between the circular disks (L) and the velocity components ($\bar{u}$, $\bar{v}$, $\bar{V}_\phi$) by the energy diffusion velocity $V_\alpha = \alpha/L$; the scales for time and pressure are, respectively, L^2/α and $\rho\alpha^2/L^2$. The non-dimensional temperature is defined as: $T = (\bar{T} - \bar{T}_c)/(\Delta\bar{T})$.

For $t > 0$, the boundary conditions on the rigid disks are the no-slip condition and the temperature conditions:

on the cold disk

$$\underline{V}(r, \phi, t) = 0; \quad T(r, \phi, t) = 0; \quad 0 \le r \le 1/A; \quad 0 \le \phi \le 2\pi \tag{6a}$$

on the hot disk

$$\underline{V}(r,\phi,t)=0;\quad T(r,\phi,t)=1;\quad 0\le r\le 1/A;\quad 0\le\phi\le 2\pi \tag{6b}$$

The boundary conditions on the free surface ($r=c(z)$) are the kinematic conditions of a stream surface (zero normal velocity), the Marangoni conditions (shear stress balance) and the adiabatic condition (the reference Marangoni number Ma is defined as $\mathrm{Ma}=\sigma_T\overline{\Delta T}\,L/\mu\alpha$) :

$$(1-c'^2)\left(\frac{\partial u}{\partial r}+\frac{\partial v}{\partial z}\right)+2c'\left(\frac{\partial v}{\partial r}-\frac{\partial u}{\partial z}\right)$$

$$=-\mathrm{Ma}\,(1+c'^2)^{1/2}\left(c'\frac{\partial T}{\partial r}+\frac{\partial T}{\partial z}\right) \tag{7a}$$

$$\frac{\partial V_\phi}{\partial r}-\frac{V_\phi}{r}+\frac{1}{r}\frac{\partial v}{\partial\phi}-c'\left(\frac{\partial V_\phi}{\partial z}+\frac{1}{r}\frac{\partial u}{\partial\phi}\right)=-\mathrm{Ma}\,(1+c'^2)^{1/2}\frac{\partial T}{\partial\phi} \tag{7b}$$

$$\frac{\partial T}{\partial r}-c'\frac{\partial T}{\partial z}=0 \tag{7c}$$

The present assumption of adiabatic free interface (equation 7(c)) is strictly related to the values assumed by the Marangoni number close to the threshold of the instability. The critical Marangoni number is in fact of the order $O(10^1\text{-}10^2)$ and the corresponding temperature difference applied along the liquid interface (according to the physical properties listed in Table II and in the case $L=1$ cm) is of the order $O(10^{-1})$ [K]. Obviously, $\bar{T}_c$ is of the same order of magnitude of the melting temperature $\bar{T}_m$ of the material under investigation ($O(10^2\text{-}10^3)$ in the case of metals). For this reason, $\overline{\Delta T}/\bar{T}_c \ll 1$ and the heat loss towards the ambient (supposed at temperature $\bar{T}_c$) can be assumed not to alter significantly the temperature field with respect to adiabatic conditions.

To solve the problem, the body-fitted curvilinear co-ordinates are adopted. The non-cylindrical original physical domain in the (r, z, ϕ) space is transformed into a cylindrical computational domain in the (ξ, η, ϕ) space by

$$\begin{array}{c} z=\xi \\ r=\eta\,c(\xi) \end{array}\quad\rightarrow\quad\begin{array}{c} \xi=z \\ \eta=r/c(\xi) \end{array} \tag{8}$$

the radial co-ordinate r ranges from $\eta=0$ (at the symmetry axis) up to $\eta=1$ at the free surface; the axial co-ordinate varies from $\xi=0$ at the bottom disk up to $\xi=1$ at the top disk. The transformed equations and boundary conditions will be found in the appendix (equations (9) and (10)).

Numerical solution

Cylindrical shape

In the case of cylindrical surface, equations 5(a)-(e) are discretized by a finite difference method with a modified central difference treatment for the convective terms and non-uniform staggered grids. Non-uniform grids are adopted to increase the resolution. The HSMAC scheme is used to proceed time evolution of velocity and pressure. For the sake of reducing computation time, the energy equation is solved by an implicit method. By this modification, computation speed is increased by a factor ranging between 3 and 10. This method becomes more effective for smaller Pr cases. Further details on the numerical method will be found elsewhere (Imaishi *et al.*, 1999, 2000; Yasushiro *et al.*, 1997, 1999, 2000).

Non-cylindrical shape

In the case of deformed shape, transformed equations are solved numerically in the (ξ, η, ϕ) space in primitive variables by a time-explicit finite-difference method (SMAC method). The transformed domain is discretized with a uniform cylindrical mesh and the flow field variables defined over a staggered grid. The axial velocity component is staggered in axial direction with respect to the point in which temperature and pressure are computed. In a similar way, the radial and azimuthal velocity components are staggered in radial and azimuthal directions, respectively.

Forward differences in time and central-differencing schemes in space (second order accurate) are used to discretize the energy and momentum partial differential equations. For further details on the numerical method see Lappa and Savino (1999) and Lappa *et al.* (2001a).

Validation of the codes

Both codes were carefully validated in previous papers by comparing the first critical Marangoni number with those of linear stability analyses in the case of cylindrical shape (Imaishi *et al.*, 1999; Lappa *et al.*, 2001a, b; Yasushiro *et al.*, 2000). Further, they have been cross-validated for the present analysis through evaluation of the first critical Marangoni number for a same reference case. Table I indicates the reliability of the numerical results by using a non-uniform mesh in radial direction in the case $\mathrm{Pr} = 0.01$, $A = 2$, $L = 1\,\mathrm{cm}$, heating from above condition, cylindrical shape. The results by the non-uniform mesh agree within 2.5 per cent to the critical Marangoni number computed by using

Table I.
Cross-check of the codes ($\mathrm{Pr} = 0.01$, cylindrical shape, on ground heating from above)

	Non-uniform mesh	Uniform mesh
Mesh	$N_Z = 38$, $N_r = 26$, $N_\phi = 43$	$N_Z = 38$, $N_r = 60$, $N_\phi = 33$
Ma_{c_1}	15.37	15.69

a uniform mesh whose size corresponds to the minimum radial step used by the non-uniform mesh.

In order to determine the growth rate constants, the Marangoni number is changed in a stepwise manner at $t = 0$. The results give the growth rate constant as a function of the Marangoni number. According to linear stability criteria (Chen and Hu, 1998; Chen *et al.,* 1997, 1999; Kuhlmann and Rath, 1993; Wanschura *et al.*, 1995), the critical Marangoni number is determined as the Marangoni number at which the growth rate becomes zero.

Results and discussion

Due to the long computational time required for the 3D simulations, the analysis has been restricted to only one value of the aspect ratio ($A = 2.0$, $L = 1$ cm) and to two different values of the Prandtl number ($\mathrm{Pr} = 0.01$ and $\mathrm{Pr} = 0.0207$) corresponding to silicon and gallium, respectively (the physical properties of these materials are listed in Table II, respectively). The simulations are carried out for heating from above, heating from below and zero g conditions in the case of cylindrical shape and for heating from above and heating from below in the case of gravity-deformed shape. This artifice (effect of gravity on the shape of the bridge ignored or "switched on") is introduced to discern the separate effects of buoyancy (bulk volume forces) and of the static deformation of the liquid/air interface (geometrical boundary condition).

The calculations were run on several Alpha-CPU based workstations and on an MPU of the Fujitsu VPP700 supercomputer at the Computer Center of Kyushu University. The grids used for the simulations are shown in Table III. The computed shape in the case of silicon (Si) and gallium (Ga) are shown in Figure 2. The corresponding value of the non-dimensional parameter k_2 for Si and Ga is 3.386 and 8.3344, respectively. Figure 2 shows that the shape of the Ga liquid bridge is more significantly deformed than that of Si because of the higher density of Ga.

	Physical properties of silicon	Physical properties of gallium
Density ρ [g/cm^3]	2.53	6.10
Thermal diffusivity α [cm^2/s]	2.44×10^{-1}	1.66×10^{-1}
Kinematic viscosity ν [cm^2/s]	2.45×10^{-3}	3.44×10^{-3}
Dynamic viscosity μ [g/cm s]	6.2×10^{-3}	2.12×10^{-2}
Prandtl number	0.01	0.0207
Thermal expansion coefficient β [1/K]	1.4×10^{-4}	1.26×10^{-4}
Surface tension σ [dyne/cm]	7.33×10^{2}	7.18×10^{2}
σ_T [dyne/cmK]	1×10^{-1}	1×10^{-1}

Table II. Physical properties of silicon and gallium

Two-dimensional analysis

Preliminary computations concerning the case of axi-symmetric Marangoni flow ($Ma < Ma_{c1}$), have been performed in order to study effects associated to the surface shape prior to the onset of complex 3D flow. As expected, the influence of the deformation of the interface on the flow field is significant even if the deviation from the straight condition is small. This behaviour can be explained according to the fact that, since the same heat flux must pass through each axial cross-section (adiabatic interface), the axial temperature gradients are directly related to the size of the cross-sectional area and, therefore, variations in the cross-sectional area must have a strong effect.

According to Figures 3-7, the surface deformation influences both temperature and velocity distributions on the free surface and the position of the vortex core in the bulk of the specimen. Figures 3 and 4 show in particular, the surface temperature distribution (a) and the surface velocity profile (b) in the case of silicon and gallium, respectively. Note that in these figures, $z = 0$

Table III.
Grids used for the computations

	Cylindrical shape non-uniform mesh	Gravity deformed shape uniform mesh
Silicon	$N_Z = 38$, $N_r = 26$, $N_\phi = 43$	$N_Z = 38$, $N_r = 60$, $N_\phi = 33$
Gallium	$N_Z = 38$, $N_r = 26$, $N_\phi = 43$	$N_Z = 38$, $N_r = 60$, $N_\phi = 49$

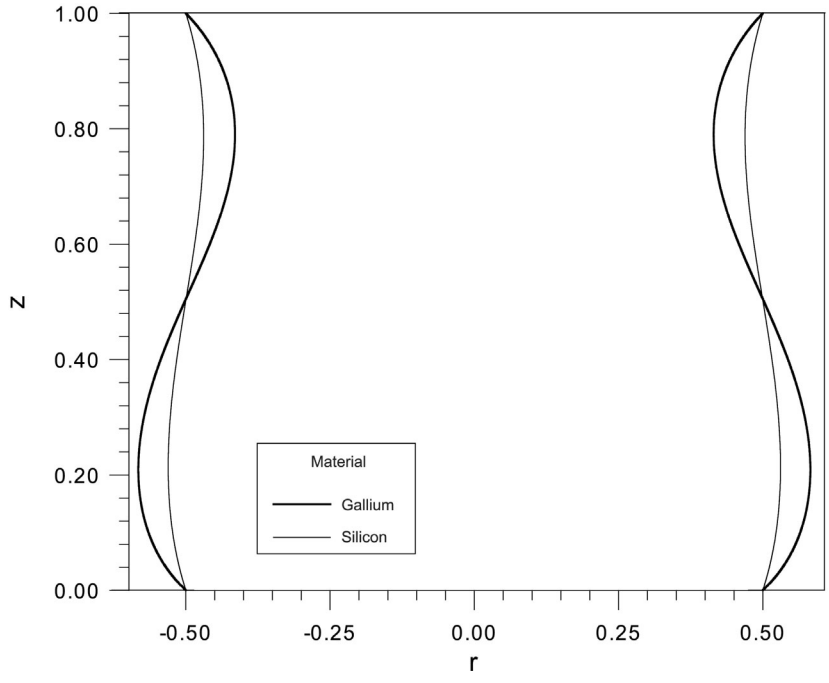

Figure 2.
Computed free surface shape

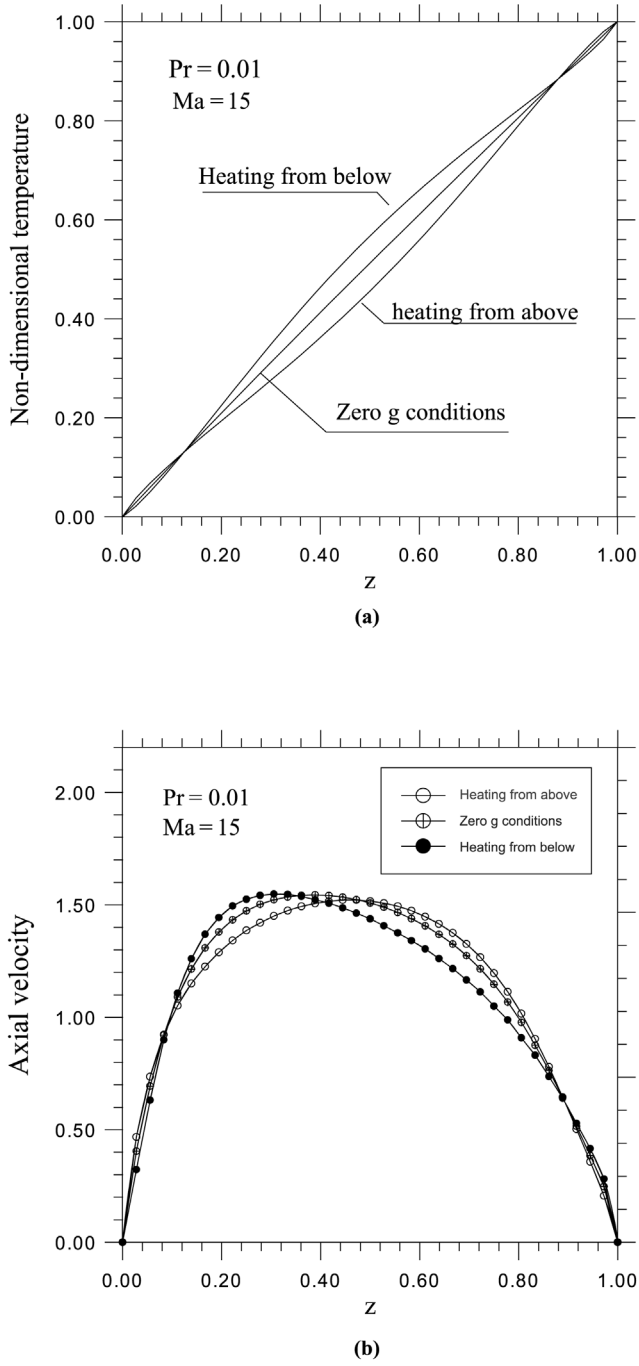

Figure 3.
Surface temperature distribution (a) and surface velocity profile (b) in the case of silicon liquid bridge

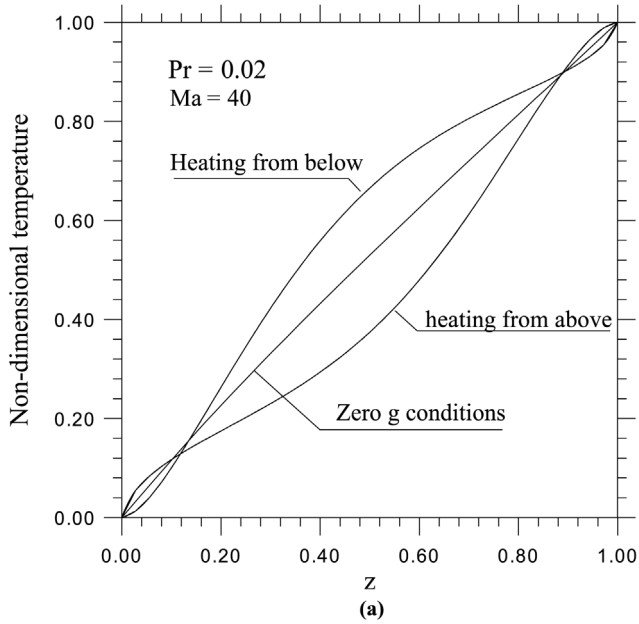

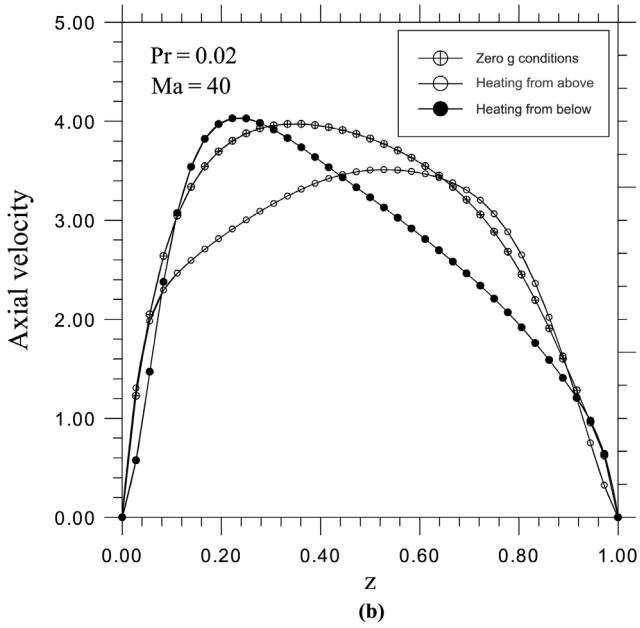

Figure 4.
Surface temperature distribution (a) and surface velocity profile (b) in the case of gallium liquid bridge

corresponds to the cold disk and $z = 1$ to the hot disk. The location of the maximum surface velocity moves towards the hot disk in the case of heating from above and towards the cold disk in the opposite case. On the contrary, the vortex core is shifted towards the cold disk in the case of heating from above and towards the hot disk if the direction of gravity is reversed (see Table IV, Figures 5-7(a); note that in Figure 7 the direction of the z axis has been reversed). Moreover, with respect to the results for the cylindrical surface, the vortex core is shifted outwards (i.e. towards the free surface) regardless of the direction of gravity (parallel or antiparallel to the axis). This effect increases the effective diameter (D_V) of the convection roll.

The above explanation highlights some interesting aspects related to the deformation of the surface; however, note that "*a priori*" predictions about the instability threshold behaviour are not possible at this stage. The influence of

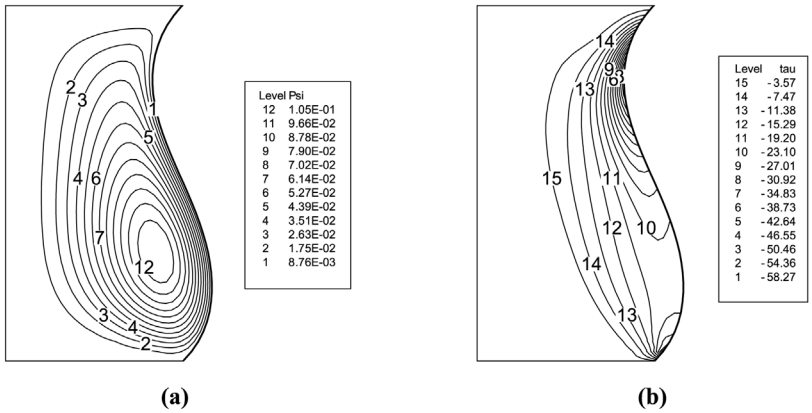

Figure 5.
Velocity distribution (a) and axial stress distribution (b) (Pr = 0.02, Ma = 40, bridge heated from above)

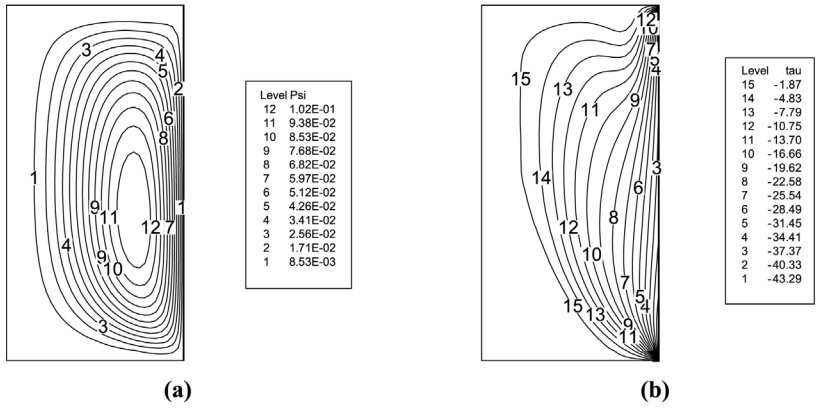

Figure 6.
Velocity distribution (a) and axial stress distribution (b) (Pr = 0.02, Ma = 40, microgravity conditions)

the free surface shape on the axial stress ($\tau = -\mu du/dr$) distribution in the bulk (responsible of the inertia instability occurring in the case of low Prandtl number liquid) is extremely complex as shown in Figures 5-7(b).

Three-dimensional simulations

Silicon liquid bridge. The 3D simulations carried out in the case of silicon show that the disturbances grow exponentially with time, i.e. $V_\phi = V_{\phi 0}\exp(\beta t)\sin(m\phi)$, and after a long incubation time macroscopic 3D steady velocity and temperature fields are established (stationary bifurcation).

In order to discern the effect of the buoyancy forces on the stability of the Marangoni flow, in the first group of calculations, the shape deformation has been neglected.

Figure 8(a) shows the values of the growth rate constants (β) obtained for different values of the Marangoni number and for different conditions (i.e. zero g conditions (Ra = 0), on ground heating from above (Ra < 0) and heating

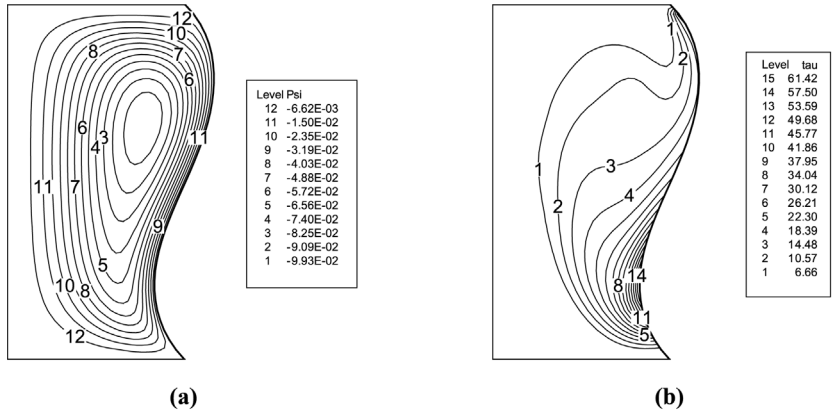

Figure 7.
Velocity distribution (a) and axial stress distribution (b) (Pr = 0.02, Ma = 40, bridge heated from below)

	Position of the vortex core	Maximum surface velocity location
Silicon liquid bridge		
Zero g	($r = 0.36$, $z = 0.425$)	$z = 0.36$
Heating from above	($r = 0.385$, $z = 0.36$)	$z = 0.48$
Heating from below	($r = 0.365$, $z = 0.55$)	$z = 0.30$
Gallium liquid bridge		
Zero g	($r = 0.36$, $z = 0.41$)	$z = 0.36$
Heating from above	($r = 0.39$, $z = 0.43$)	$z = 0.56$
Heating from below	($r = 0.365$, $z = 0.66$)	$z = 0.23$

Table IV.
Position of the vortex core and maximum surface velocity location in the case of silicon liquid bridge and gallium liquid bridge

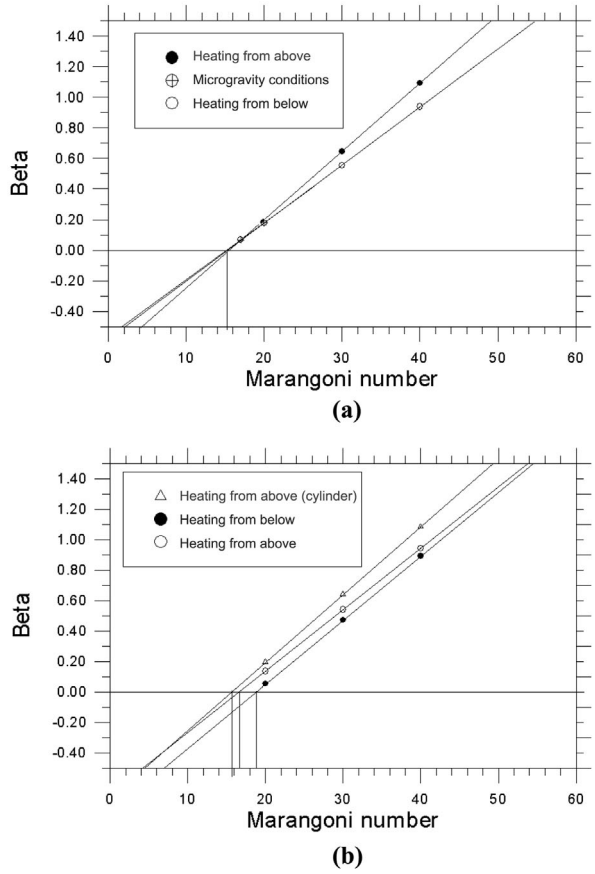

Figure 8.
Growth rates as function of the Marangoni number and determination of the first critical Marangoni number. (a) Cylindrical shape, silicon liquid bridge; (b) gravity-deformed shape, silicon liquid bridge

from below (Ra $>$ 0)). The growth rates obtained in the case of normal gravity conditions and heating from above (Ra $<$ 0) lie below the corresponding ones obtained in the case of microgravity conditions (Ra $=$ 0). Viceversa, the growth rates obtained in the case heating from below are above those corresponding to zero g conditions. For the different cases, the wave number is always equal to one ($m = 1$) thus showing that in the case of a silicon liquid bridge having a length of 1 cm and $A = 2$, the azimuthal wave number is not affected by the buoyancy forces. According to the behaviour of the evaluated growth rates, the on ground critical Marangoni numbers in the case of heating from above ($Ma_{c1} = 15.36$) and heating from below ($Ma_{c1} = 14.92$) are increased and decreased, respectively, with respect to the case of microgravity conditions ($Ma_{c1} = 15.24$) (Table V).

As a second step, in order to elucidate the overall effect of the gravity field (i.e. buoyancy forces + surface deviation from the straight configuration), the

deformation of the shape has been taken into account. According to the results in Figure 8(b), the growth rates obtained in the case of heating from above and deformed shape lie below the corresponding ones obtained in the case of cylindrical shape thus giving rise to a stabilization of the flow field ($Ma_{c1} = 16.62$). Despite the different value of the critical Marangoni number ($Ma_{c1} = 16.62$ instead of $Ma_{c1} = 15.36$) this trend is similar to that already discussed for the cylindrical case. However, contrary to the case of straight surface, if the surface deformation is not ignored, the flow exhibits further stabilization for the heating from below condition. The corresponding values of the growth rate in fact are below those obtained in the opposite case ($Ma_{c1} = 18.78$).

According to these results, if the liquid bridge is allowed to deform, gravity always acts stabilizing the Marangoni flow regardless of its direction (parallel or antiparallel to the axis).

The direction, however, is crucial in determining the azimuthal organization. The structures of the flow and temperature fields in fact are characterized by $m = 1$ in the case of heating from below and $m = 2$ if the direction of gravity is reversed. The different azimuthal structures of the thermofluid-dynamic field at the steady state, according to the gravity level and according to the heating condition (from above and from below) are shown in Figures 9 and 10.

Note that the azimuthal velocity maxima on the free surface always occur near the cold disk. This behaviour is in agreement with the results of the linear stability analysis of Wanschura *et al.* (1997). In their analysis, the radial flow near the cold disk was supposed to have an important role for the mechanism of amplification of the disturbances leading to the instability. Moreover, note that the influence of the buoyancy forces on the values of the growth rates and, therefore, on the critical Marangoni number in the case of cylindrical shape can be explained on the basis of their results. Wanschura *et al.* (1997) found in fact that the efficiency of the process of amplification of the azimuthal disturbances responsible of the inertia instability is proportional to the radial gradient of the base state axial velocity, i.e. the axial shear. Marangoni forces driving the basic flow field induce a strong axial shear flow close to the free melt/air interface. The higher the intensity of the axial share, the lower should be the critical Marangoni number.

Table V.
Critical Marangoni number

	Cylinder 1*g* heating from above	Cylinder Zero *g*	Cylinder 1*g* heating from below	1*g* shape heating from above	1*g* shape heating from below
Silicon	15.36	15.24	14.92	16.62	18.78
Gallium	36.19	33.78	31.87	89.51	242.2

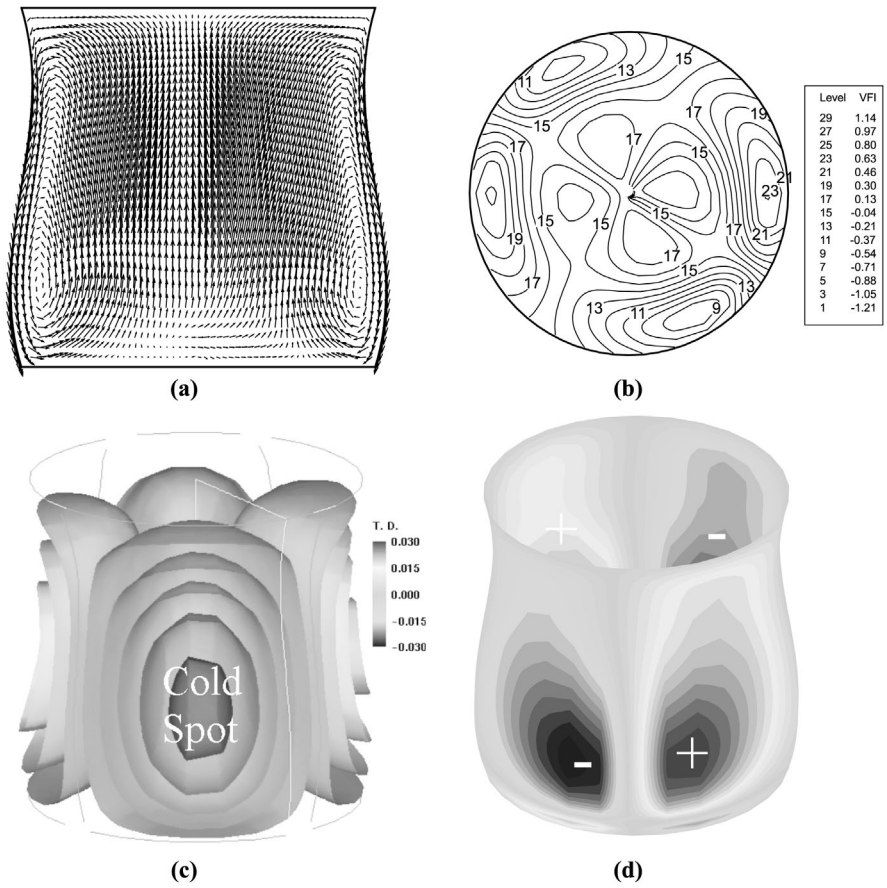

Figure 9.
Structure of 3D Marangoni flow with $m = 2$ in the case of silicon liquid bridge, $\mathrm{Ma} = 40$ at the steady state, 1 , bridge heated from above. (a) Velocity field in the meridian plane $\phi = 3\pi/4$; (b) azimuthal velocity in the cross-section $z = 0.5$; (c) 3D view of the iso-surfaces of the temperature disturbance; (d) azimuthal velocity on the free surface

According to this theory, the stabilization of the flow field in the case of heating from above follows from the decrease of the surface axial shear intensity that in this case is reduced since buoyancy and Marangoni forces counteract on the free interface.

Nevertheless, this theory cannot be used to draw general conclusions about the stabilization mechanisms. The present simulations in fact highlight that, if the gravity-deformation of the surface is taken into account, both the heating conditions (from above and from below) stabilize the flow field. In this case the stabilization with respect to zero g conditions is not trivial. However, a possible explanation could be related to the increase of the diameter of the convection roll (pointed out in the paragraph "two-dimensional analysis") associated to the deformation of the shape. In fact, due to the increase of this diameter, the effective aspect ratio of the toroidal vortex is reduced.

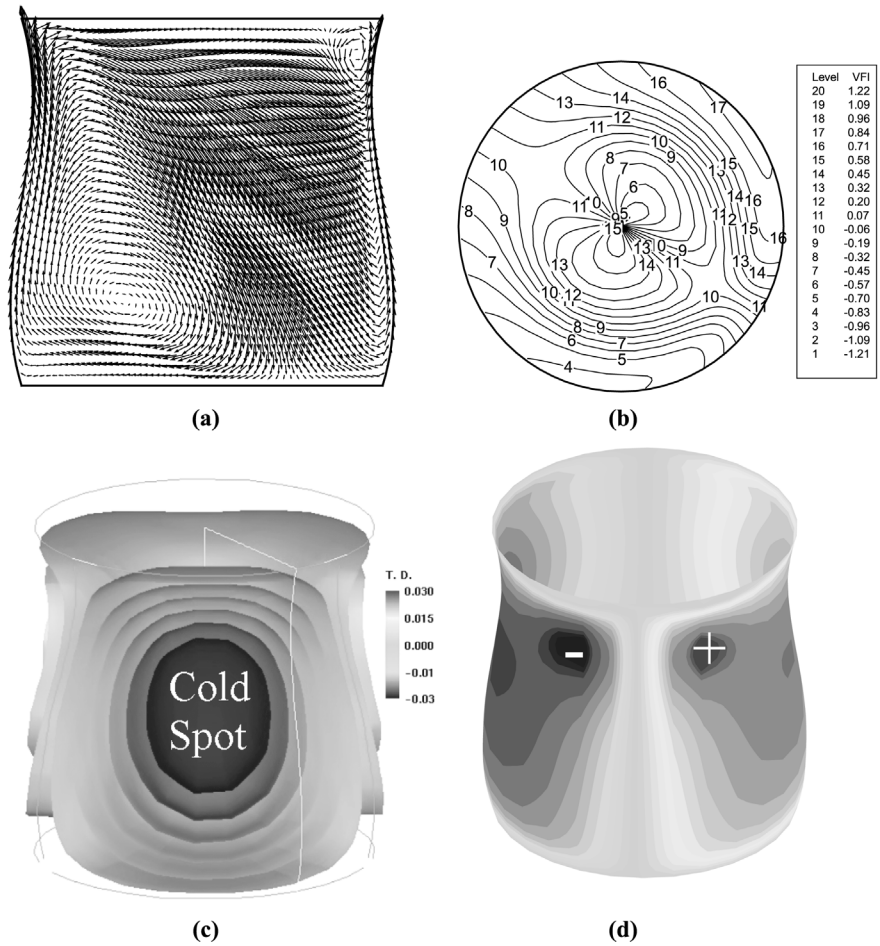

Figure 10.
Structure of 3D Marangoni flow with $m = 1$ in the case of silicon liquid bridge, $\mathrm{Ma} = 40$ at the steady state, 1g, bridge heated from below. (a) Velocity field in the meridian plane $\phi = 3\pi/4$; (b) azimuthal velocity in the cross-section $z = 0.5$; (c) 3D view of the iso-surfaces of the temperature disturbance; (d) azimuthal velocity on the free surface

Gallium liquid bridge

The values of the growth rate constants yielded for different values of the Marangoni number and for different conditions in the case of cylindrical free surface are shown in Figure 11. The trend is similar to that discussed in the case of silicon. The critical Marangoni numbers are $\mathrm{Ma}_{c1} = 33.78$ in the case of zero g conditions and $\mathrm{Ma}_{c1} = 36.19$ and $\mathrm{Ma}_{c1} = 31.87$ under 1g for heating from above and below, respectively. For these cases the wave number is always equal to one ($m = 1$).

If the deformation of the shape is not ignored, a very complex scenario arises. In the case of heating from above the most dangerous azimuthal wave number is $m = 2$. The value of the critical Marangoni number ($\mathrm{Ma}_{c1} = 89.51$, Figure 12(a)) is significantly increased with respect to the cases where the straight surface is assumed ($m = 1$ and $\mathrm{Ma}_{c1} = 36.19$).

It is known that discrete wavenumbers of disturbances are selected out of the full spectrum of disturbances because the convection roll is closed in a special zone geometry. If the instability is hydrodynamic in nature, since it does not depend on the behaviour of the temperature field (for this instability, the temperature field simply acts as a driving force for the velocity field), the selection rule is given simply by the constraint that the azimuthal wavelength must be an aliquot of the toroidal vortex core circumference and by the fact that the convection roll is limited axially by the presence of the sidewalls (Lappa *et al.*, 2001a). According to this theory, the critical wave number is related to the axial length of the zone and to the diameter D_V of the center-line of the convection roll, i.e. it scales with the parameter $A_V = 2L/D_V$. Thus, the selection of a higher value ($m = 2$) of the azimuthal wave number as most dangerous disturbance (leading to a higher value of the critical Marangoni number) in the case of gallium liquid bridge, can be explained by the fact that due to the large deformation of the free surface, the liquid zone held between the supporting disks behaves as a lower aspect ratio bridge (Table IV). This theory is supported by the new findings by Imaishi *et al.* (2001) for cylindrical liquid bridge of low Pr fluids, i.e. in the range of $A > 1.2$, a shorter cylindrical liquid bridge requires the larger temperature difference for the first flow transition and the most dangerous mode is $m = 2$ for $1 < A < 1.8$ (Figure 13).

If the direction of gravity is reversed (heating from below), the value of the critical Marangoni number is increased up to $\mathrm{Ma_c} = 242.2$ (Figure 12(b)). Note that no steady bifurcation occurs in this case and the instability threshold value is much higher than the second critical Marangoni number for a cylindrical liquid bridge of $\mathrm{Pr} = 0.02$ fluid ($\mathrm{Ma_{c_2}} = 131.8$ for $g = 0$). The flow becomes unstable against 3D disturbances directly through a Hopf bifurcation characterized by a value of the azimuthal wave number $m = 1$ and critical frequency $f = 0.31$ Hz (obtained by an extrapolation). Moreover,

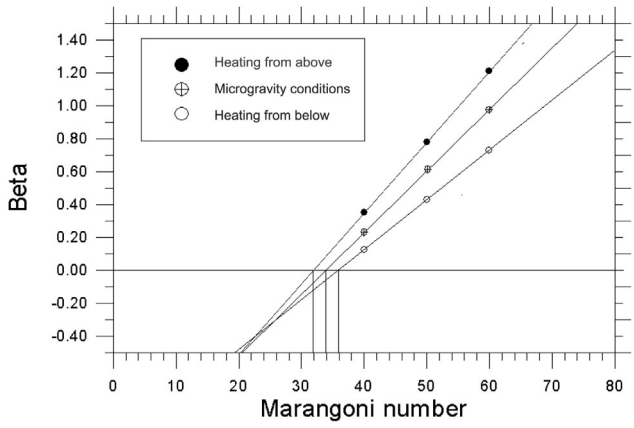

Figure 11.
Growth rates as a function of the Marangoni number and determination of the first critical Marangoni number (cylindrical shape, gallium liquid bridge)

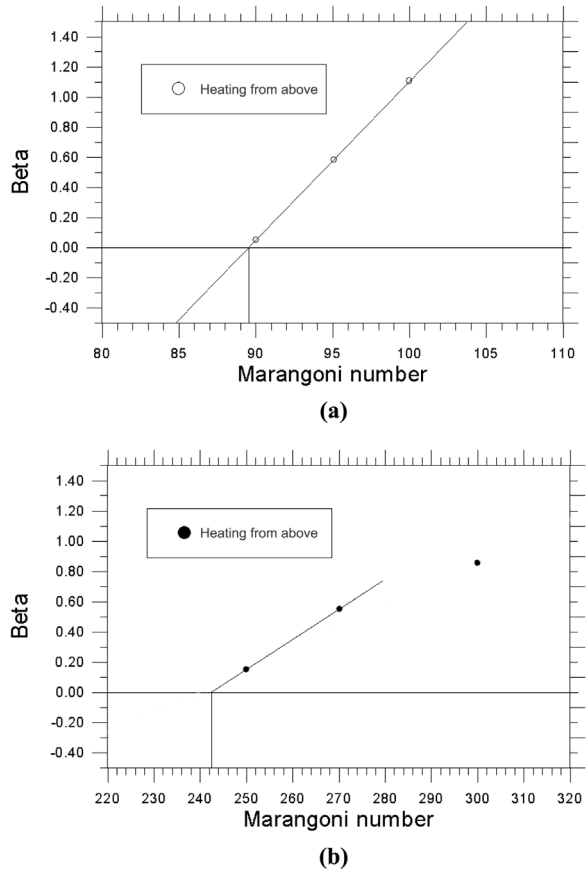

Figure 12.
Growth rates as a function of the Marangoni number and determination of the first critical Marangoni number (on ground deformed shape, gallium liquid bridge)

the numerical simulations highlight that the spatio-temporal behaviour is quite different with respect to the case of the second bifurcation of flow in a liquid bridge of low Prandtl number fluid already depicted in detail in previous works (Imaishi *et al.*, 1999, 2000; Levenstan and Amberg, 1995; Leypoldt *et al.*, 2000). In those cases, oscillatory flow is superimposed on a steady 3D field established through the first flow transition. The present study uncovers a new, heretofore unseen transition directly from steady to oscillatory flow without the intermediate state of steady, asymmetric flow traditionally computed for the low-Pr case.

Figure 14 shows the time evolution of the maximum surface azimuthal velocity obtained for Ma = 300. At early stage, during a transient unsteady phase ($t < 10.4$), the spatio-temporal behaviour is "rotating". The temperature disturbances on the interface (surface temperature spots) rotate around the

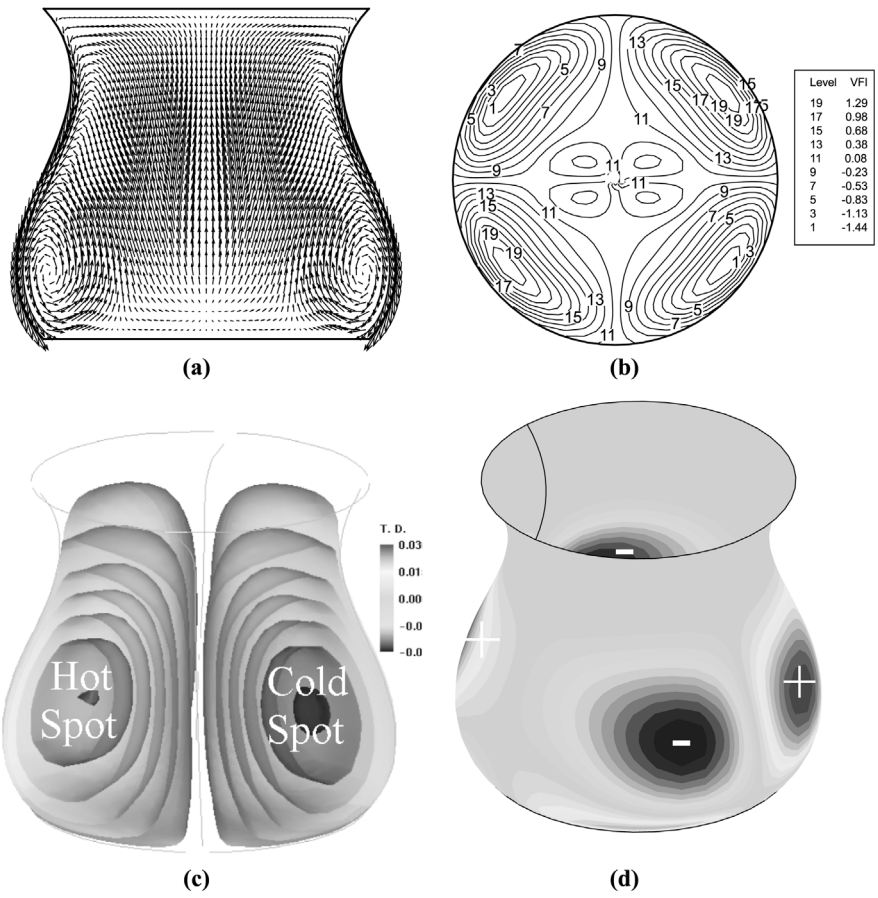

Figure 13.
Structure of 3D Marangoni flow with $m = 2$ in the case of gallium liquid bridge, $\mathrm{Ma} = 120$ at the steady state, $1g$, bridge heated from above. (a) Velocity field in the meridian plane $\phi = 0$; (b) azimuthal velocity in the cross-section $z = 0.5$; (c) 3D view of the iso-surfaces of the temperature disturbance; (d) azimuthal velocity on the free surface

perimeter of the liquid bridge (Figure 15, the period τ has been divided into four parts and the temperature field is shown in Figure 15(a)-(d), corresponding to $t = 0, \tau/4, \tau/2, 3\tau/4$). The time dependent behaviour of the temperature field is simply characterized by a full rotation of the entire flow pattern in azimuthal direction (Figure 16).

After a transient phase, the early rotating regime is taken over by a new spatio-temporal behaviour (Figure 14). During the rotating regime, the frequency is $f = 0.449\,\mathrm{Hz}$ but after a transient time the frequency becomes $f = 0.386\,\mathrm{Hz}$. In this case, the behaviour is "pulsating". The pulsating temperature spots on the surface of the bridge are shown in Figure 17 (the period τ has been divided into four parts and the fields are shown in Figure 17(a)-(d) corresponding to $t = 0,\ \tau/4,\ \tau/2,\ 3\tau/4$). These temperature spots "pulsate", i.e. the cold spot grows in axial direction during the shrinking

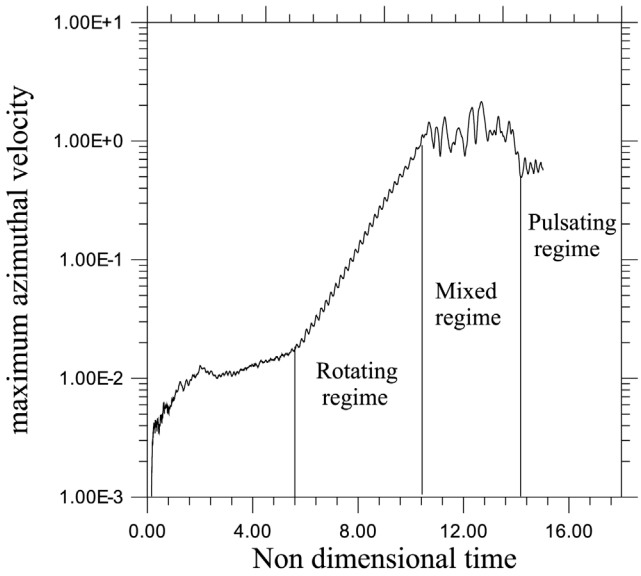

Figure 14.
Time evolution of the maximum surface azimuthal velocity in the case of gallium liquid bridge, Ma = 300, 1*g*, heating from below

of the hot spot and viceversa but, the azimuthal positions of these extrema do not change (Figure 18).

To further clarify these behaviours and to establish a simple criterion to "detect" the oscillating regime (to be used during experimental investigations), four "numerical" thermocouples have been located in the bridge (Figure 19) having the same axial and radial co-ordinates ($r = 1/A, z = 0.75$) but different azimuthal positions (with a shift of 90°). In Figure 20, the computed temperatures of the thermocouples T_1, T_2, T_3 and T_4, are shown for the "rotating regime". Figure 21 shows the results obtained for the "pulsating regime".

During the early transient stage dominated by the "rotating" behaviour, the amplitude of the temperature oscillations does not depend on the local azimuthal position of the thermocouples and is the same for all the points having the same radial and axial position. In this transient stage the surface spots are not fixed, but rotate in azimuthal direction, hence each of the four numerical thermocouples measures a maximum (minimum) temperature value when the hot (cold) spot passes on it. In the rotating model, the time temperature profiles show hence a phase displacement depending on the azimuthal co-ordinate. Since the critical wave number is $m = 1$, the oscillations show a phase displacement of $\pi/2$ between two numerical thermocouples located at angular distance of 90° and a phase displacement of π between two numerical thermocouples located at angular distance of 180°. For the "pulsating regime", there is no phase shift between T_1 and T_4 and no phase shift between T_2 and T_3 but T_1 and T_4 measure values with a phase shift of π

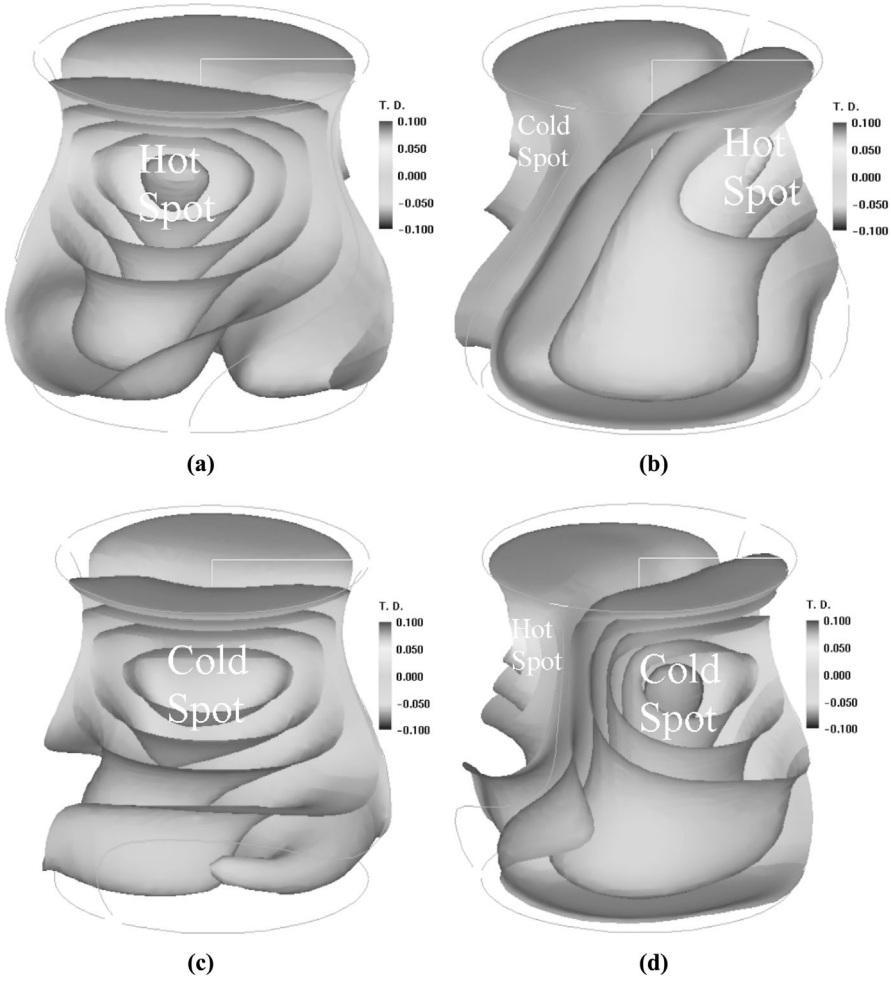

Figure 15.
Snapshots of temperature disturbance iso-surfaces over a period of oscillation (Ma = 300, deformed shape, heating from below, rotating regime)

with respect to T_2 and T_3. This behaviour comes from the fact that the temperature disturbance can be represented as two spots on the liquid bridge surface. In the pulsating model, these spots have azimuthal fixed positions. Since for $m = 1$, the azimuthal extension of each spot is 180°, and the thermocouples have an azimuthal shift of 90°, two thermocouples will be placed on a spot and the others on the second spot measuring values having an opposite phase.

Moreover, other distinguishing marks between the two regimes can be highlighted: in the "pulsating" regime, the "numerical" probes located on the free surface at the same axial position with an angular shift of 90°, do not measure the same maximum neither the same minimum (i.e. the amplitudes of

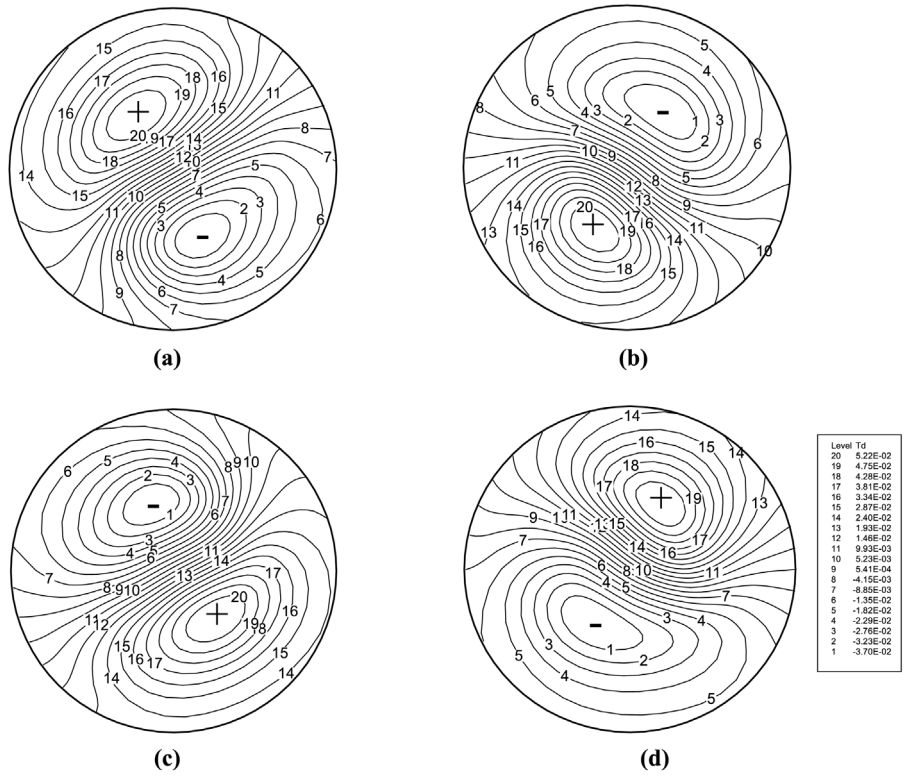

Figure 16.
Snapshots of temperature disturbances at $z = 0.5$ over a period of oscillation (Ma = 300, deformed shape, heating from below, rotating regime)

the oscillations measured by the thermocouples are different). This behaviour occurs since the azimuthal position of the spots is fixed and the azimuthal temperature distribution related to each spot is not uniform, i.e. each thermocouple measures a maximum (minimum) value of the temperature depending on its local azimuthal position on the spot.

Though the similarity of this oscillatory flow with Marangoni flow instabilities in the case of high Prandtl number liquids (standing waves and travelling waves (Lappa *et al.*, 2001b; Yasushiro *et al.*, 1997, 1999), the mechanism of the instability observed in the present results is completely different. In fact, the azimuthal flow is not driven by the surface temperature distribution. On the free surface, the azimuthal flow is directed from the cold spot towards the hot spot (azimuthal flow due to the instability and azimuthal Marangoni effect "counteract" on the free surface), thus proving that in this case the instability is hydrodynamic in nature.

Finally Figure 22 shows the oscillatory behaviour of the temperature field for the case of cylindrical liquid bridge heated from below (Ra $>$ 0) at Ma = 160,

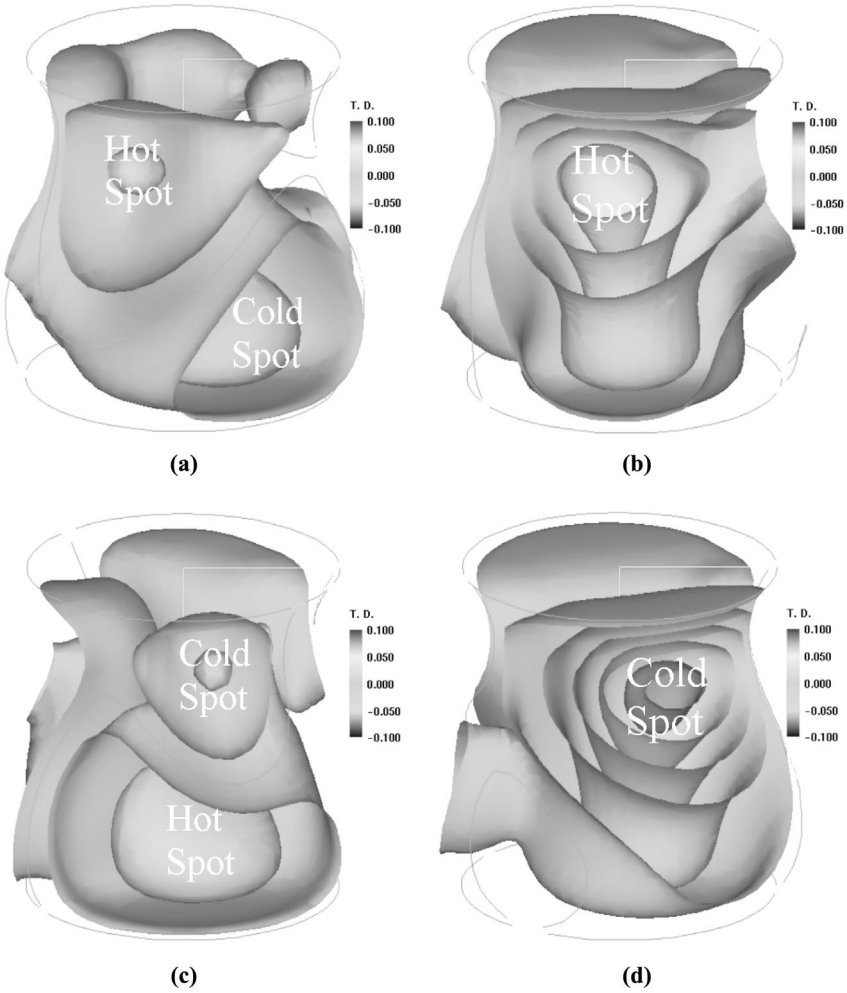

Figure 17.
Snapshots of temperature disturbance iso-surfaces over a period of oscillation (Ma = 300, deformed shape, heating from below, pulsating regime)

slightly above the second critical Marangoni number under micro gravity condition ($Ma_{c_2} = 131.8$). In this case a "torsional" oscillatory motion with $m = 1$ is dominant. The wave number is the same as that in a deformed liquid bridge, but the oscillatory behaviour is completely different being characterized by a periodic twist (back and forth motion) in azimuthal direction of the 3D $m = 1$ disturbance.

Conclusions

The influence of the gravity effect on the features of the Marangoni flow instability in half zone liquid bridges in the case of low Prandtl liquids has

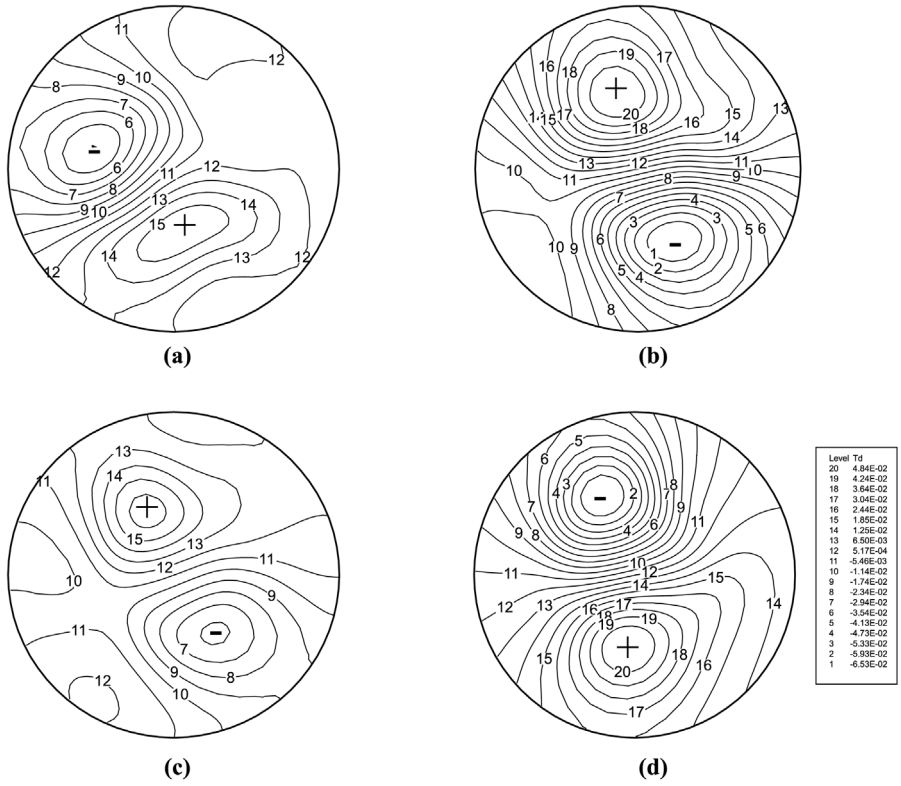

Figure 18.
Snapshots of temperature disturbances at $z = 0.5$ over a period of oscillation (Ma = 300, deformed shape, heating from below, pulsating regime)

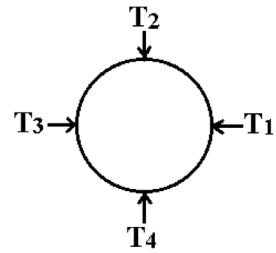

Figure 19.
Azimuthal position of the four numerical "probes"

been investigated by direct 3D and time-dependent simulation of the problem. This topic is important since most of the available experimental data come from on ground experimentation. The simulation have been carried out for heating from above, heating from below and zero g conditions in the case of cylindrical shape (gravity deformation "switched off") and for heating from above and heating from below in the case of melt/gas interface allowed to deform.

For the latter situation, body-fitted curvilinear co-ordinates have been adopted; the non-cylindrical original physical domain in the (r, z, ϕ) space has been transformed into a cylindrical computational domain in a (ξ, η, ϕ) space. Silicon and gallium liquid bridges ($L = 1$ cm, $A = 2.0$) have been investigated. The computed shape of the liquid bridges exhibit different behaviour according to the physical properties of the melts. The interface of the Gallium liquid bridge is strongly deformed whereas in the case of silicon, the deviation from the cylindrical surface is small.

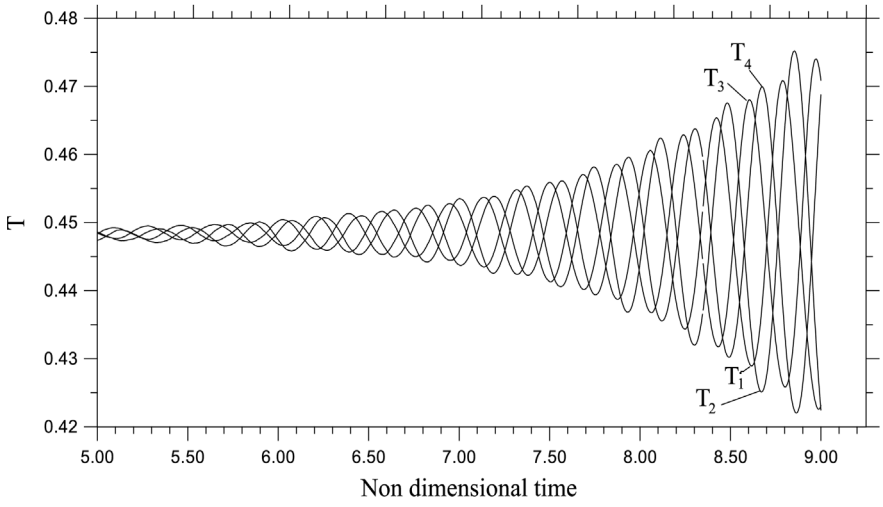

Figure 20.
Time evolution of the temperatures measured by four numerical "probes" located at different azimuthal positions with a shift of 90° (free surface, $z = 0.75$) during the "rotating regime" (gallium liquid bridge, 1g, Ma = 300, heating from below)

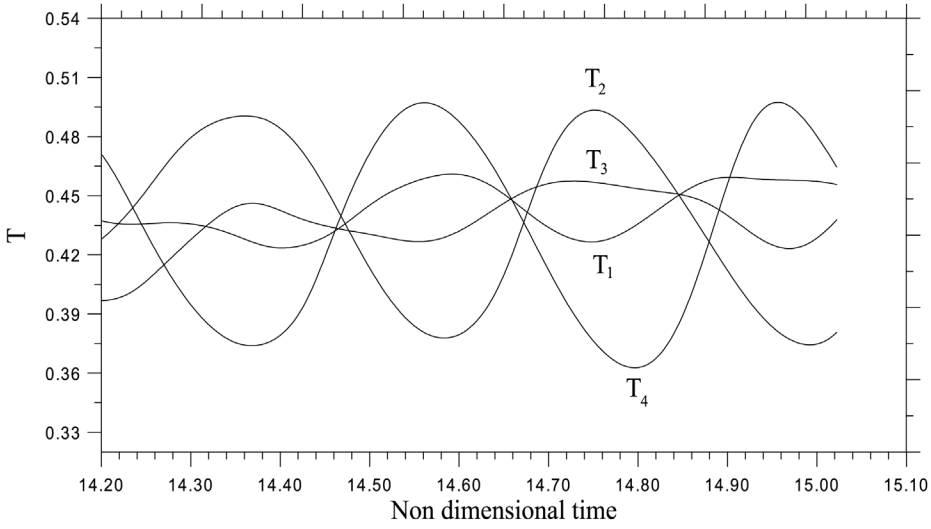

Figure 21.
Time evolution of the temperatures measured by four numerical "probes" located at different azimuthal positions with a shift of 90° (free surface, $z = 0.75$) during the "pulsating regime" (gallium liquid bridge, 1g, Ma = 300, heating from below)

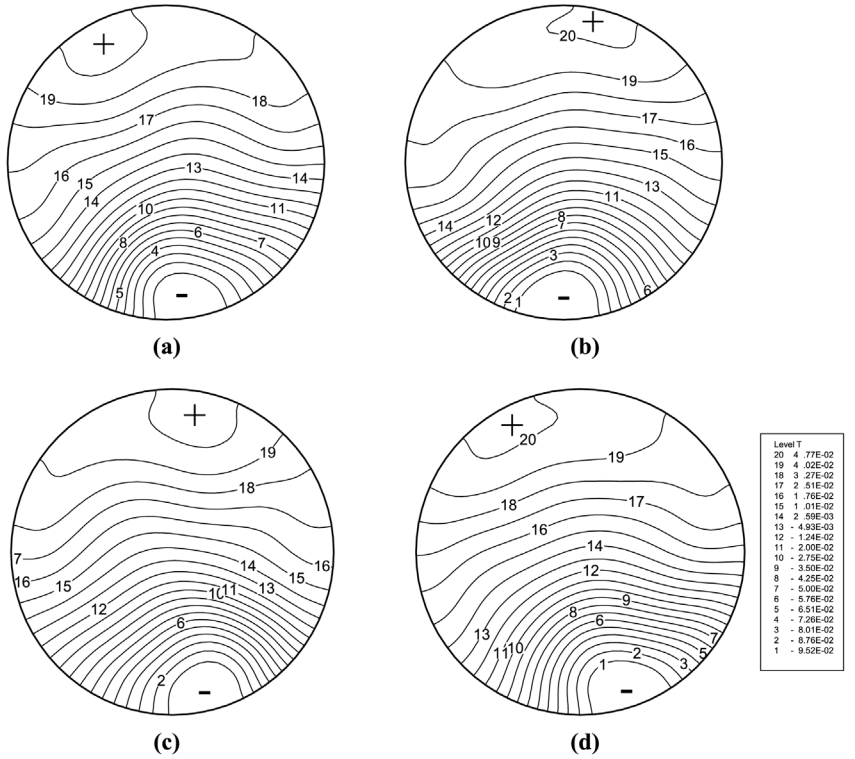

Figure 22.
Snapshots of temperature disturbances at $z = 0.5$ over a period of oscillation (gallium liquid bridge, 1g, Ma = 160, heating from below, cylindrical interface)

In the case of straight surface, the growth rates obtained under normal gravity and heating from above conditions lie below the corresponding ones obtained in the case of microgravity environment. Viceversa, the growth rates obtained in the case heating from below are above those corresponding to zero g conditions. For the different cases, the wave number is always equal to one ($m = 1$) thus showing that in the case of a silicon and gallium liquid bridges having a length of 1 cm, the azimuthal flow structure is not affected by the buoyancy forces. The on ground critical Marangoni numbers in the case of g parallel and antiparallel to the bridge axis are increased and decreased, respectively, with respect to the case of microgravity conditions.

If the deformation of the shape is not ignored, the flow exhibits further stabilization for the heating from below condition. The corresponding values of the growth rate in fact lie below those obtained in the opposite case. Therefore, in real liquid bridges, gravity always acts stabilizing the Marangoni flow regardless of its direction.

The on ground static shape also influences the value of the azimuthal organization of the flow field. The wave number is shifted to higher values if

the heating from above condition and the deformation of the free surface are taken into account.

The stabilization and destabilization of the flow field for the different configurations have been explained according to the process of selection and amplification of the azimuthal disturbances responsible for the inertia instability. In the case of heating from below and cylindrical interface, in particular, the destabilization follows from the increase of intensity of the axial shear associated to the combined effect of buoyancy and Marangoni forces on the free surface. On the other hand, if the surface is allowed to deform, the stabilization occurring for both the heating conditions (from above and from below) is related to the increase of the diameter of the convection roll. In fact, due to the increase of this diameter, the effective aspect ratio of the toroidal vortex is reduced.

In the case of heating from below, a surprising behaviour has been found in the case of gallium. The axi-symmetric steady flow is strongly stabilized and maintained up to $\mathrm{Ma}_c = 242.2$. At this Marangoni number, there arises a direct transition to 3D oscillatory flow with $m = 1$ and critical frequency 0.31 Hz. This value is significantly larger than the second critical Marangoni number value for a cylindrical liquid bridge under microgravity condition, i.e. $\mathrm{Ma}_{c_2} = 131.8$. The critical threshold is increased and surprisingly, no steady bifurcation occurs. The flow becomes unstable to 3D disturbances directly through a Hopf (oscillatory) bifurcation. The present study uncovers a new, heretofore unseen, transition from steady to oscillatory flow without the intermediate state of steady, asymmetric flow traditionally computed for the low-Pr case. The instability behaves as a high-Pr-like oscillatory bifurcation. The spatio-temporal behaviour of the flow field is "rotating" during an early stage and then this regime is taken over by a "pulsating" regime. Though the similarity with hydrothermal instabilities is already observed in the case of high Prandtl number liquid, this oscillatory bifurcation has been proved to be hydrodynamic in nature and has never been reported before. Further investigation is required to investigate these aspects from an experimental point of view. For this reason, some experimental criterions to detect the transition from one regime to the other have been suggested and discussed.

According to the present analysis, the liquid bridge exhibits different behaviours according to the level of detail used to model the effect of gravity (static deformation neglected or "switched off"). The difference between the straight and the deformed configuration and the related possibility to use one or the other model to better reproduce the behaviours of on ground floating zones used for the crystal growth process have been investigated and discussed in detail. Contrary to the case of high Prandtl number liquids, for the present case, the effect of buoyancy forces does not seem to play an important role whereas the shape is crucial in determining the stability properties of the flow (i.e. the critical Marangoni number) and its 3D structure (i.e. the azimuthal wave

number) as well as the type of bifurcation (steady or oscillatory). The paper introduces novel results and, at the same time, represents a quite exhaustive attempt to help investigators to discern the complex interrelations among various effects and in particular, those associated to the presence of gravity.

References

Chen, Q.S. and Hu, W.R. (1998), "Influence of liquid bridge volume on instability of floating half-zone convection", *Int. J. Heat Mass Transfer*, Vol. 41, pp. 825-37.

Chen, Q.S., Hu, W.R. and Prasad, V. (1999), "Effect of liquid bridge volume on the instability in small-Prandtl-number half zones", *Journal of Crystal growth*, Vol. 203, pp. 261-8.

Chen, G., Lizee, A. and Roux, B. (1997), "Bifurcation analysis of the thermocapillary convection in cylindrical liquid bridges", *Journal of Crystal growth*, Vol. 180, pp. 238-47.

Frank, S. and Schwabe, D. (1998), "Temporal and spatial elements of thermocapillary convection in floating zones", *Experiments in Fluids*, Vol. 23, pp. 234-51.

Imaishi, N., Yasuhiro, S., Akiyama, Y. and Yoda, S. (2001), "Numerical simulation of oscillatory Marangoni flow in half-zone liquid bridge of low Prandtl number fluid", *J. Crystal Growth*, Vol. 230, pp. 164-71.

Imaishi, N., Yasushiro, S., Sato, T. and Yoda, S. (1999), "Three dimensional numerical simulation of oscillatory Marangoni flow in a half zone of low Pr fluids", *Material Research in Low Gravity II*, SPIE, The International Society for Optical Engineering, 19-21 July 1999, Denver, Colorado, Vol. 3792, pp. 344-52.

Imaishi, N., Yasushiro, S., Sato, T. and Yoda S. (2000), "Numerical simulation of three dimensional oscillatory flow in half zone bridges of low Pr fluid", *Proceedings 292 of the 4th JSME-KSME Thermal Engineering Conference*, 1-6 October 2000, Kobe, Japan, pp. 272-82.

Kuhlmann, H.C. and Rath, H.J. (1993), "Hydrodynamic instabilities in cylindrical thermocapillary liquid bridges", *J. Fluid Mech.*, Vol. 247, pp. 247-74.

Lappa, M. and Savino, R. (1999), "Parallel solution of three-dimensional Marangoni flow in liquid bridges", *Int. J. Num. Meth. Fluids*, Vol. 31, pp. 911-25.

Lappa, M., Savino, R. and Monti, R. (2000), "Influence of buoyancy forces on Marangoni flow instabilities in liquid bridges", *Int. J. Num. Meth. Heat Fluid Flow*, Vol. 10 No. 7, pp. 721-49.

Lappa, M., Savino, R. and Monti, R. (2001a), "Three-dimensional numerical simulation of Marangoni instabilities in non-cylindrical liquid bridges in microgravity", *Int. J. Heat Mass Transfer*, Vol. 44 No. 10, pp. 1983-2003.

Lappa, M., Savino, R. and Monti, R. (2001b), "Three-dimensional numerical simulation of Marangoni instabilities in liquid bridges: influence of geometrical aspect ratio", *Int. J. Num. Meth. Fluids*, Vol. 36 No. 1, pp. 53-90.

Levenstam, M. and Amberg, G. (1995), "Hydrodynamical instabilities of thermocapillary flow in a half-zone", *J. Fluid Mech.*, Vol. 297, pp. 357-72.

Leypoldt, J., Kuhlmann, H.C. and Rath, H.J. (2000), "Three-dimensional numerical simulation of thermocapillary flows in cylindrical liquid bridges", *J. Fluid Mech*, Vol. 414, pp. 285-307.

Nakamura, S., Hibiya, T., Kakimoto, K., Imaishi, N., Nishizawa, S.-I., Hirata, A., Mukai, K., Yoda, S.-I. and Morita, T.S. (1998), "Temperature fluctuations of the Marangoni flow in a liquid bridge of molten silicon under microgravity on board the TR-I4 rocket", *Journal of Crystal Growth*, Vol. 186, pp. 85-93.

Neitzel, G.P., Chang, K.T., Jancowski, D.F. and Mittelmann, H.D. (1992), "Linear stability of thermocapillary convection in a model of the float-zone crystal-growth process", *Phys. Fluids A*, Vol. 5, pp. 108-14.

Preisser, F., Schwabe, D. and Scharmann, A. (1983), "Steady and oscillatory thermocapillary convection in liquid columns with free cylindrical surface", *J. Fluid Mech.*, Vol. 126, pp. 545-67.

Rupp, R., Muller, G. and Neumann, G. (1989), "Three dimensional time dependent modelling of the Marangoni convection in zone melting configurations for GaAs", *Journal of Crystal Growth*, Vol. 97, pp. 34-41.

Shevtsova, V.M. and Melnikov, D.E. (2000), "Influence of variable viscosity on convective flow in liquid bridges. 3-D simulations of ground based experiments", *1st Symposium on Microgravity Research and Applications in Physical Science and Biotechnology*, September 2000, Sorrento, Italy.

Velten, R., Schwabe, D. and Scharmann, A. (1991), "The periodic instability of thermocapillary convection in cylindrical liquid bridges", *Phys. Fluids A*, Vol. 3, pp. 267-79.

Wanschura, M., Kuhlmann, H.C. and Rath, H.J. (1997), "Linear stability of two-dimensional combined buoyant-thermocapillary flow in cylindrical liquid bridges", *Physical Review E*, Vol. 55 No. 6, pp. 7036-42.

Wanschura, M., Shevtsova, V., Kuhlmann, H.C. and Rath, H.J. (1995), "Convective instability mechanism in thermocapillary liquid bridges", *Phys. Fluids*, Vol. 5, pp. 912-25.

Yasushiro, S., Sato, T. and Imaishi, N. (1997), "Three dimensional oscillatory Marangoni flow in a half zone of Pr = 1.02 fluid", *Microgravity Sci. Technol.*, Vol. X/3, pp. 144-53.

Yasushiro, S., Imaishi, N., Kuhlmann, H.C. and Yoda, S. (1999), "Numerical simulation of three dimensional oscillatory thermocapillary flow in a half zone of Pr = 1 fluid", *Adv. Space Res.*, Vol. 24, pp. 1385-90.

Yasushiro, S., Sato, T., Imaishi, N. and Yoda, S. (2000), "Three dimensional Marangoni flow in liquid bridge of low Pr fluid", *Space Forum*, Vol. 6, pp. 39-47.

Zeng, Z., Mizuseki, H., Higashino, K. and Kawazoe, Y. (1999), "Direct numerical simulation of oscillatory Marangoni convection in cylindrical liquid bridges", *Journal of Crystal Growth*, Vol. 204, pp. 395-404.

Appendix: equations and boundary conditions in body fitted co-ordinates

$$\frac{\partial u}{\partial \xi} - \frac{c'}{c}\eta\frac{\partial u}{\partial \eta} + \frac{1}{c}\frac{\partial v}{\partial \eta} + \frac{v}{\eta c} + \frac{1}{\eta c}\frac{\partial V_\phi}{\partial \phi} = 0 \tag{9a}$$

$$\begin{aligned}\frac{\partial u}{\partial t} = &-\left(\frac{\partial P}{\partial \xi} - \frac{c'}{c}\eta\frac{\partial P}{\partial \eta}\right) - \left(\frac{\partial u^2}{\partial \xi} - \frac{c'}{c}\eta\frac{\partial u^2}{\partial \eta} + \frac{1}{c}\frac{\partial uv}{\partial \eta} + \frac{uv}{\eta c} + \frac{1}{\eta c}\frac{\partial uV_\phi}{\partial \phi}\right)\\ &+ \mathrm{Pr}\left[\frac{\partial^2 u}{\partial \xi^2} + \left(\left(\frac{c'}{c}\eta\right)^2 + \frac{1}{c^2}\right)\frac{\partial^2 u}{\partial \eta^2} - 2\frac{c'}{c}\eta\frac{\partial^2 u}{\partial \xi \partial \eta} + \left(\frac{1}{\eta c^2} + 2\left(\frac{c'}{c}\right)^2\eta - \frac{c''}{c}\eta\right)\frac{\partial u}{\partial \eta} + \frac{1}{\eta^2 c^2}\frac{\partial^2 u}{\partial \phi^2}\right]\\ &- \mathrm{Pr}\,\mathrm{Ra}\,T\end{aligned} \tag{9b}$$

$$\frac{\partial v}{\partial t}=-\left(\frac{1}{c}\frac{\partial P}{\partial \eta}\right)-\left(\frac{\partial uv}{\partial \xi}-\frac{c'}{c}\eta\frac{\partial uv}{\partial \eta}+\frac{1}{c}\frac{\partial v^2}{\partial \eta}+\frac{v^2}{\eta c}-\frac{V_\phi^2}{\eta c}+\frac{1}{\eta c}\frac{\partial vV_\phi}{\partial \phi}\right)$$
$$+\mathrm{Pr}\left[\frac{\partial^2 v}{\partial \xi^2}+\left(\left(\frac{c'}{c}\eta\right)^2+\frac{1}{c^2}\right)\frac{\partial^2 v}{\partial \eta^2}-2\frac{c'}{c}\eta\frac{\partial^2 v}{\partial \xi\partial \eta}+\left(\frac{1}{\eta c^2}+2\left(\frac{c'}{c}\right)^2\eta-\frac{c''}{c}\eta\right)\frac{\partial v}{\partial \eta}\right. \quad (9c)$$
$$\left.-\frac{v}{\eta^2c^2}+\frac{1}{\eta^2c^2}\frac{\partial^2 v}{\partial \phi^2}-\frac{2}{\eta^2c^2}\frac{\partial V_\phi}{\partial \phi}\right]$$

$$\frac{\partial V_\phi}{\partial t}=-\left(\frac{1}{c\eta}\frac{\partial P}{\partial \phi}\right)-\left(\frac{\partial uV_\phi}{\partial \xi}-\frac{c'}{c}\eta\frac{\partial uV_\phi}{\partial \eta}+\frac{1}{c}\frac{\partial vV_\phi}{\partial \eta}+\frac{2vV_\phi}{\eta c}+\frac{1}{\eta c}\frac{\partial V_\phi^2}{\partial \phi}\right)$$
$$+\mathrm{Pr}\left[\frac{\partial^2 V_\phi}{\partial \xi^2}+\left(\left(\frac{c'}{c}\eta\right)^2+\frac{1}{c^2}\right)\frac{\partial^2 V_\phi}{\partial \eta^2}-2\frac{c'}{c}\eta\frac{\partial^2 V_\phi}{\partial \xi\partial \eta}+\left(\frac{1}{\eta c^2}+2\left(\frac{c'}{c}\right)^2\eta-\frac{c''}{c}\eta\right)\frac{\partial V_\phi}{\partial \eta}\right.$$
$$\left.-\frac{V_\phi}{\eta^2c^2}+\frac{1}{\eta^2c^2}\frac{\partial^2 V_\phi}{\partial \phi^2}+\frac{2}{\eta^2c^2}\frac{\partial v}{\partial \phi}\right] \quad (9d)$$

$$\frac{\partial T}{\partial t}=-\left(\frac{\partial uT}{\partial \xi}-\frac{c'}{c}\eta\frac{\partial uT}{\partial \eta}+\frac{1}{c}\frac{\partial vT}{\partial \eta}+\frac{vT}{\eta c}+\frac{1}{\eta c}\frac{\partial V_\phi T}{\partial \phi}\right)$$
$$+\left[\frac{\partial^2 T}{\partial \xi^2}+\left(\left(\frac{c'}{c}\eta\right)^2+\frac{1}{c^2}\right)\frac{\partial^2 T}{\partial \eta^2}-2\frac{c'}{c}\eta\frac{\partial^2 T}{\partial \xi\partial \eta}+\left(\frac{1}{\eta c^2}+2\left(\frac{c'}{c}\right)^2\eta-\frac{c''}{c}\eta\right)\frac{\partial T}{\partial \eta}+\frac{1}{\eta^2c^2}\frac{\partial^2 T}{\partial \phi^2}\right] \quad (9e)$$

At the interface:

$$\left(\frac{1+c'^2}{c}\right)\frac{\partial u}{\partial \eta}-2c'\frac{\partial u}{\partial \xi}+\left(\frac{c'+c'^3}{c}\right)\frac{\partial v}{\partial \eta}+(1-c'^2)\frac{\partial v}{\partial \xi}=-\mathrm{Ma}(1+c'^2)^{1/2}\frac{\partial T}{\partial \xi} \quad (10a)$$

$$(1+c'^2)\frac{\partial V_\phi}{\partial \eta}-cc'\left(\frac{\partial V_\phi}{\partial \xi}+\frac{1}{c}\frac{\partial u}{\partial \phi}\right)-V_\phi+\frac{\partial v}{\partial \phi}=-\mathrm{Ma}\,(1+c'^2)^{1/2}\frac{\partial T}{\partial \phi} \quad (10b)$$

$$\left(\frac{1}{c}+\frac{c'^2}{c}\right)\frac{\partial T}{\partial \eta}-c'\frac{\partial T}{\partial \xi}=0 \quad (10c)$$